Plasmonic interactions between a metallic nanoshell and a thin metallic film

F. Le,[1] N. Z. Lwin,[2] N. J. Halas,[2,3] and P. Nordlander[1,3,*]
[1]*Department of Physics and Astronomy, M.S. 61, Rice University, Houston, Texas 77005-1892, USA*
[2]*Department of Chemistry, M.S. 60, Rice University, Houston, Texas 77005-1892, USA*
[3]*Department of Electrical and Computer Engineering, M.S. 366, Laboratory for Nanophotonics, Rice University, Houston Texas 77005-1892, USA*

(Received 20 July 2006; revised manuscript received 19 August 2007; published 8 October 2007)

The plasmonic interaction and optical properties of a metallic nanoshell near a metallic film are investigated theoretically and experimentally. The plasmon hybridization method is extended to include the screening effects mediated by dielectric backgrounds and a realistic description of the dielectric properties of the metal. We show that the plasmonic structure of the system depends strongly on the aspect ratio of the nanoshell (the ratio of inner to outer radius) and the thickness of the film. In the thin film limit, the plasmonic coupling between the nanoshell and the film induces a low-energy virtual state (VS) mainly consisting of delocalized thin film plasmons. We show that the energy and intensity of this state can both be controlled by the aspect ratio of the nanoshell and the thickness of the film. The theoretical results are found to agree well with experimental observations. Using finite-difference time-domain simulations, we show that the electromagnetic field enhancements induced by excitation of the VS can be very large and that the nanoshell/thin film system could serve as a tunable plasmonic substrate for surface enhanced spectroscopies.

DOI: 10.1103/PhysRevB.76.165410 PACS number(s): 73.20.Mf, 78.68.+m, 78.30.−j

I. INTRODUCTION

The optical properties of macroscopic and mesoscopic metallic structures are of considerable importance in both fundamental and applied science.[1–3] Applications such as chemical and biosensing, for example, are beginning to exploit surface enhanced Raman spectroscopy, where the excitations of nanoparticle plasmons in a nanostructure-based substrate can provide large enhancements of the local electromagnetic field and drastically increase the Raman cross section of adsorbed molecules.[4–10] Other applications include the development of ultrasmall waveguides depending on subwavelength plasmonic structures as potential optical interconnects in computer chips.[11–16]

The energies of the plasmon resonances of nanoparticles depend sensitively on their composition and shape.[17–25] In nanoparticle aggregates such as dimers, the plasmon resonances depend strongly on interparticle separations.[26–32] For nanoparticles near semi-infinite metallic surfaces, the plasmon resonances have been shown to depend strongly on nanoparticle-surface separation.[33–37] The plasmon resonances have been found to depend strongly on interparticle separations in nanoparticle arrays of various dimensionalities.[38–42]

In a recent paper, we showed that the metallic nanosphere/film system represents a highly tunable plasmonic nanostructure, where the plasmon energies can depend sensitively on the ratio of nanoparticle radius to the thickness of the film.[43] We showed that the plasmonic interactions in the system are described by a model analogous to the standard impurity models such as the spinless Anderson-Fano model. The discrete and localized nanoparticle plasmons interact with the continuum of delocalized film plasmons, an interaction that can result in localized states, resonances, and virtual states (VSs) in the continuum. These concepts were originally introduced to describe the nature of the electronic states resulting from the interaction of a discrete impurity level with a continuum,[44] and have also been used to describe the interaction of localized and delocalized photonic states in photonic crystals.[45] The VS is a state composed primarily of continuum states with only a small admixture of the discrete state, in contrast to the localized state, which is primarily composed of the discrete state. Both the localized state and VS were identified experimentally, and the tunability of the VS was observed in a series of systematic experiments, where metallic nanospheres were deposited, along with a constant-thickness spacer layer, onto metallic films of decreasing thickness.[43] In a subsequent paper, the finite-difference time-domain (FDTD) method was used to study the electromagnetic properties of the VS.[46] It was shown that the VS is characterized by a strong coupling between the nanosphere and the film, with large field enhancements induced in the junction between the nanosphere and the nearest film surface.

In this paper, we generalize our method to include the effects of dielectric backgrounds and a realistic description of the metals and apply our method to a metallic nanoshell outside a thin metallic film. In contrast to a solid nanosphere, the nanoshell is in itself a highly tunable metallic nanoparticle consisting of a thin metallic shell around a spherical dielectric core.[17] The discrete plasmon resonances of a nanoshell depend strongly on its aspect ratio x, the ratio of inner shell radius a to outer shell radius b, and can be tuned across the visible and infrared regions of the spectrum. Thus, the nanoshell/film system can exhibit a higher tunability than the nanosphere on a film. For a low aspect ratio nanoshell where the discrete nanoshell plasmon resonances lie above the effective film continuum (the regime inside the film plasmonic band that strongly interacts with the nanoparticle[46]), we find a localized plasmon resonance above the continuum and a broad VS in the continuum. For a nanoshell of intermediate aspect ratio, where the discrete nanoshell resonances lie within the film continuum, the finite probability of plasmon hopping into the film results in a broadening of the

plasmon resonances. For a nanoshell of large aspect ratio, the virtual state is further tuned into the low-energy part of the film plasmon continuum. Our calculated optical spectra compare well with experimental measurements. Using FDTD, we investigate the electric field enhancements induced by excitations of the plasmon modes and show that these enhancements can be very large. Our study shows that the nanoshell/thin film system exhibits greater tunability and larger electromagnetic field enhancements than the nanosphere/film system.

The organization of the paper is as follows. In Sec. II, we present the generalization of the plasmon hybridization (PH) method to the metallic nanoshell/film system and show how dielectric background effects can be included in the formalism. In Sec. III, we present the calculated plasmonic structure and compare it with results from FDTD simulations and experimental measurements. In Sec. IV, we discuss the results and present the major conclusions of the study.

II. THEORY

The physical situation being modeled is that of the discrete plasmons of a finite metallic nanoshell interacting with a continuum of delocalized surface plasmons of a directly adjacent metallic film of finite thickness. In the PH method,[47,48] the plasmons are modeled as incompressible deformations of the electron gas of the particle on top of a uniform, rigid background of positive charge. The kinetic energy of the time-dependent deformations is balanced by a force resulting from the potential energy of the spill-out charges at the surfaces of the nanostructure. The potential energy is calculated using the instantaneous Coulomb potential. Since the method is nonretarded, it applies rigorously only to nanostructures of dimensions much smaller than the wavelength of incident light. This condition is satisfied in the present problem because the interactions between the film and the nanoparticle are mediated by nonretarded film plasmons of wavelengths comparable to the size of the nanoparticle.[37,43]

To describe the plasmons of the interacting system, the charge deformations are expanded in a complete set of primitive plasmons associated with the elementary surfaces of the system.[47] The primitive plasmons interact and hybridize with each other, forming bonding and antibonding plasmons in direct analogy with molecular orbital theory. The method provides an intuitive understanding of how the geometrical and structural properties of a nanostructure influence its plasmon resonances, and agrees very well with simulations performed using computational approaches such as the fully retarded FDTD method.[48]

In the following, we assume a uniform conduction electron density n_S in the nanoshell and n_F in the film. These densities will enter the formalism in terms of the corresponding bulk plasmon energies $\omega_{B,S}=\sqrt{4\pi e^2 n_S/m_e}$ and $\omega_{B,F}=\sqrt{4\pi e^2 n_F/m_e}$. The nanoshell has an inner radius a and an outer radius b. The aspect ratio of the nanoshell is $x=a/b$. The film is assumed to have a thickness T and the separation between the center of the nanoshell and the upper surface of the film is denoted Z_0. The width of the junction between the nanoshell and the upper film surface is $H=Z_0-b$. These geometric variables are sketched in Fig. 1. We will also include the effect of dielectric backgrounds, such as the dielectric background permittivity of the metals, ϵ_M, representing the polarizability of the metallic ions. The resulting dielectric function of the metal has a Drude form $\epsilon(\omega)=\epsilon_M(\omega)-\omega_B^2/\omega^2$. When the optical absorption of the structure is calculated, we add a damping term $i\delta(\omega)$ to the frequency. This damping describes the energy dissipation in the system and results in a complex dielectric function of the form $\epsilon(\omega)=\epsilon_M(\omega)-\omega_B^2/[\omega+i\delta(\omega)]^2$. The real parameters $\epsilon_M(\omega)$ and $\delta(\omega)$ can be fitted straightforwardly to measure real and imaginary parts of the dielectric function of Au (Ref. 49) to provide an accurate description of the dielectric properties of Au over all frequencies of interest. The specific dielectric backgrounds that will be included are illustrated in Fig. 1.

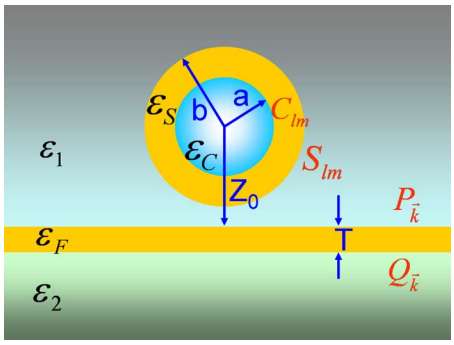

FIG. 1. (Color online) The geometry of the nanoshell-film system. Geometric variables a, b, T, and Z_0 represent the inner and outer radii of the nanoshell, the metallic film thickness, and the shell-film separation, respectively. C_{lm}, S_{lm}, $P_{\vec{k}}$, and $Q_{\vec{k}}$ are the amplitudes of the primitive nanoshell cavity, sphere plasmons, and the film plasmons on both sides. ϵ_C, ϵ_S, ϵ_1, ϵ_2, and ϵ_F are the background dielectric constants of the nanoshell core, the nanoshell metallic layer, the embedding media above and below the film, and the metallic film, respectively. The effects of varying the dielectric background constants are investigated in Fig. 4.

The deformation field associated with the plasmons can be obtained from a scalar potential η,[47] which for the present system takes the form

$$\eta = \int \frac{d\vec{k}}{(2\pi)^2} \dot{P}_{\vec{k}}(t) e^{i\vec{k}\cdot\vec{\rho}+kz} + \int \frac{d\vec{k}}{(2\pi)^2} \dot{Q}_{\vec{k}}(t) e^{i\vec{k}\cdot\vec{\rho}-k(z+T)} + \sum_{l,m} \left[\sqrt{\frac{1}{lb^{2l+1}}} \dot{S}_{lm}(t) r^l + \sqrt{\frac{a^{2l+1}}{l+1}} \dot{C}_{lm}(t) r^{-l-1} \right] Y_{lm}(\Omega). \tag{1}$$

The radial coordinate r is defined in a spherical coordinate system centered on the nanoshell and with a polar axis oriented perpendicularly to the upper film surface. The quantities Y_{lm} are the spherical harmonics. $P_{\vec{k}}$ and $Q_{\vec{k}}$ are the amplitudes of the primitive film surface plasmons associated with the surfaces closest and furthest from the nanoshell. The quantities S_{lm} and C_{lm} are the amplitudes for the primitive sphere and cavity plasmons of the nanoshell. The first two

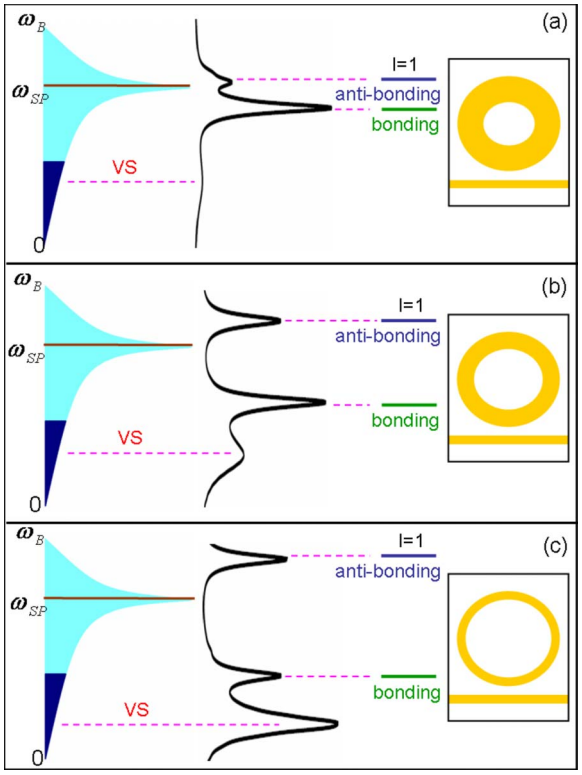

FIG. 2. (Color online) [(a)–(c)] Schematic illustration of the nanoshell-metallic film interaction as the aspect ratio ($x=a/b$) of the nanoshell increases. The light blue area to the left represents the plasmonic density of states of the film $\rho(\omega)$. The dark blue area represents the effective continuum $\rho V_{l=1}^2(\omega)$. The right part illustrates the geometry and energy of the discrete nanoshell plasmon. The black curves depict the absorption spectrum resulting from the plasmonic interaction between the nanoshell and the film.

integrals are over the two-dimensional wave vectors describing the primitive film plasmons and the two summations are over the discrete multipolar plasmonic levels of the nanoshell.

In Appendix A, it is shown how one can exploit the cylindrical symmetry of the problem and transform the primitive plasmon basis into a more convenient form. The resulting Lagrangian is diagonal in azimuthal index m and can be written as

$$L^m = \sum_{l,i=\pm} [\dot{N}_{lm,i}^2 - \omega_{l,i}^2(x) N_{lm,i}^2] + \sum_{j=\pm} \int dk [\dot{M}_j^2(k,m) - \omega_{k,j}^2(T) M_j^2(k,m)] - \sum_l \sum_{i=\pm,j=\pm} \int dk N_{lm,i} M_j(k,m) V_{lk,i,j}^m(Z_0,T). \quad (2)$$

In this expression, $N_{lm,\pm}$ represent the tunable discrete bonding $(-)$ and antibonding $(+)$ plasmon modes of an isolated nanoshell of aspect ratio x with energies $\omega_{l,\pm}(x)$ given by Eq. (A1). The amplitudes $M_\pm(k,m)$ describe the continuum of bonding $(-)$ and antibonding $(+)$ plasmons of an isolated metallic film with energies $\omega_{k,\pm}(T)$ given by Eq. (A8). With the present use of cylindrical symmetry, plasmons polarized perpendicularly to the surface are described by $m=0$ and plasmons polarized parallel to the surface correspond to $m=\pm 1$.

This Lagrangian represents a classical impurity problem, i.e., the interaction between discrete localized states with a continuum of delocalized states. The interaction $V_{lk,i,j}^m(Z_0)$ corresponds to the hopping element. The parameter describing the nature of the interaction is the effective continuum $\rho V_l^2(\omega)$, where ρ is the density of states of the bare film plasmon continuum and ω is the energy (frequency). Our previous study showed that the spectral structure of the VS is similar to that of the effective continuum.[46] In chemical terms, the VS can be viewed as a "bonding" many-particle state resulting from the interaction of a finite continuum with a higher-energy discrete state. In physical terms, it can be described as an incomplete image response to an oscillating dipole.[43] In the present paper, we will investigate thin metallic films where the effective continuum forms a broad band in the low-energy region of the film plasmon density of states.[43] In our discussion, we will focus on the dipolar $l=1$ couplings although higher multipolar couplings are present and induce a hybridization of the primitive nanoshell plasmon modes.

Since the plasmon energies of a nanoshell are dependent on its aspect ratio x, we can tune the discrete nanoshell plasmons to arbitrary positions within the effective continuum. In Fig. 2, we illustrate schematically how the interaction changes as the aspect ratio of the nanoshell is increased. The light blue areas to the left show the plasmonic density of states of the individual film, and the dark blue areas denote the lower-energy band of the effective continuum $\rho(\omega)V_{l=1}^2(\omega)$, representing the film plasmons that couple strongly to the discrete, dipolar bonding plasmon of the nanoshell. The effective continuum peaks at an energy around $\omega_{k=3/2R,-}(T)$ (Ref. 46) and extends continuously down to zero energy. The higher-energy branch of the effective continuum only interacts weakly with the bonding plasmons of the nanoshell and is therefore not highlighted in the figure. On the right, we show the location of the discrete dipolar plasmon energies of the nanoshell. Panel (a) shows the interaction for a thick nanoshell. The nanoshell plasmon lies above the effective continuum (as in the case of a nanosphere outside a thin film). The interaction results in a localized state above the continuum and a VS in the continuum. Panel (b) shows the interaction for a nanoshell of intermediate aspect ratio. Here, the energy of the discrete nanoshell plasmon falls within the effective continuum and becomes a broadened resonance. In panel (c), we show the interaction for a thin nanoshell where the VS gets pushed further to lower energies.

We discretize the continuum and introduce a vector notation which is described in Appendix B. The Lagrangian can be represented in a quadratic form

$$L^m = \frac{1}{2}\dot{\vec{X}}^T \hat{T}_X \dot{\vec{X}} - \frac{1}{2}\vec{X}^T \hat{V}_X \vec{X}, \quad (3)$$

where $\vec{X}$ is a vector representing the primitive plasmon amplitudes and $\hat{T}_X$ and $\hat{V}_X$ are matrices representing the kinetic

and potential energies of the primitive plasmon in the $\vec{X}$ basis. The superscript T denotes the transpose of a vector or matrix. In Appendix C, we show how the effects of dielectric backgrounds can be included in the formalism. Background dielectrics have no effect on the kinetic energy of the primitive plasmons but modify the potential energy matrix $\hat{V}_X$ [Eq. (C2)].

The application of the Euler-Lagrange equations results in a linear equation system from which the plasmon energies of the interacting system are obtained as eigenvalues,

$$\omega^2(\hat{T}_X + \hat{T}_X^T) - (\hat{V}_X + \hat{V}_X^T) = 0. \quad (4)$$

III. RESULTS

This section contains three subsections. In the first subsection, we present the results obtained from the PH approach. Then, we focus on the aspect-ratio dependence of the nanoshell and show how it increases the tunability of the VS. We also investigate the effects of background dielectrics on the plasmonic structure of the system. In the second subsection, we compare the PH results with results from FDTD simulations. We also present an investigation of the local electromagnetic field enhancements in the junction between the nanoshell and the film. In these two theory subsections, we use smaller nanoshells of varying inner radii but with a fixed outer radius of $b=50$ nm. We use a small nanoshell to minimize the computational effort and to enable a more direct comparison between PH and FDTD. In the third subsection, we present the experimentally measured extinction spectra of the system and compare with theoretical calculations. The gold nanoshell studied and modeled here has an inner radius of $a=60$ nm and an outer radius of $b=70$ nm.

A. Plasmon hybridization

In Fig. 3, we show the optical absorption spectra calculated for perpendicular polarization ($m=0$) for the systems that correspond to the situations depicted in Fig. 2. We only consider optical absorption by the nanoshell and neglect optical absorption in the film. This figure illustrates the shift to lower energies of the discrete nanoshell plasmon with increasing aspect ratio $x=a/b$. In each panel, the solid curve is the spectrum of the nanoshell-film system and the dashed line is for the individual nanoshell only. The spectra in the top panel are dominated by the localized state around 2.4 eV. A broad VS is observed on the low-energy side of the localized state. The small shoulder around 2.5 eV is the antibonding dipolar nanoshell plasmon, which is strongly damped and broadened due to interband transitions. For small aspect ratios, the splitting of the bonding and antibonding nanoshell plasmons is very small.[47] The middle panel shows a situation where the discrete bonding nanoshell resonance is shifted into resonance with the effective continuum. The result is a formation of a resonance which is broadened relative to the discrete nanoshell resonance. The antibonding resonance remains as a broad shoulder around 2.5 eV. In the lower panel where the discrete nanoshell state is shifted further down into the continuum, a VS appears at even lower energy and the intensity of the VS gets significantly stronger than that of the localized state. The reversal of the relative intensities of the localized peak at higher energy and the VS at lower energy from panel (b) to panel (c) does not mean a higher admixture of the discrete state into the VS. A careful analysis of the eigenvectors of the lowest-energy peak shows that the film states still dominate the mode, and thus they remain VSs. [Further evidence for this will be presented in Fig. 5(c) where the electromagnetic field enhancements for the low-energy peak display the strong coupling between the particle and the film which is characteristic of a VS.] For a thinner film, the VS would be shifted to lower energies.[43] The figure clearly demonstrates the additional tunability that is introduced by absorbing a nanoshell rather than a nanosphere on the film.[43]

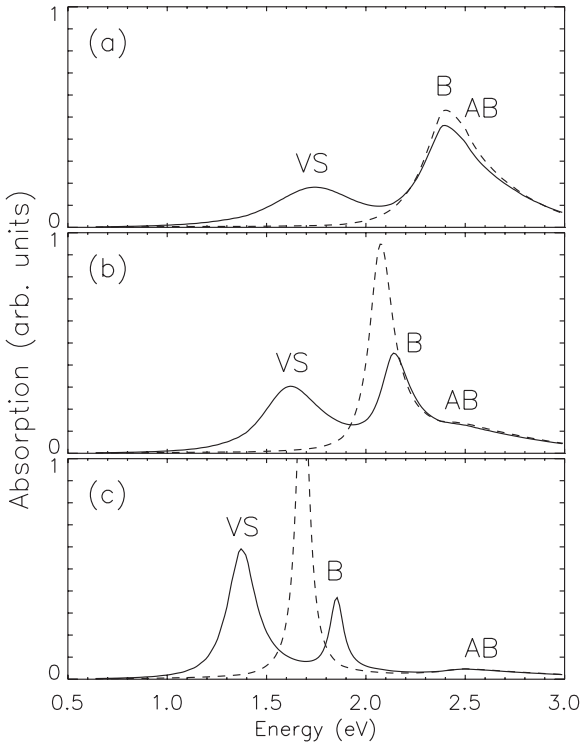

FIG. 3. Optical absorption spectra of the Au nanoshell-thin film system in geometries corresponding to Fig. 2. The solid lines are dipolar optical absorption as a function of frequency for a nanoshell of outer radius $b=50$ nm and different inner radii $a=20$ nm [panel (a)], $a=40$ nm [panel (b)], and $a=45$ nm [panel (c)]. The center of the nanoshell is at a position $Z_0=53$ nm outside a metallic film of thickness $T=12$ nm. The gold metal is modeled using Johnson-Christy data (Ref. 49) and $\epsilon_C=2.04$ (SiO_2), $\epsilon_1=1$ (air), and $\epsilon_2=2.25$ (glass). The dotted lines are the absorption spectra for the individual nanoshells. The peaks labeled "VS" are the virtual states. The peaks labeled "B" and "AB" are the discrete dipolar bonding and antibonding nanoshell peaks, respectively. The antibonding peaks are strongly damped and broadened due to interband transitions.

In Fig. 4, we investigate the effect of dielectric backgrounds on the absorption spectrum of the nanoshell/film system. Panel (a) shows the spectra for a Au film in vacuum. A VS appears around 1.5 eV and the localized state around

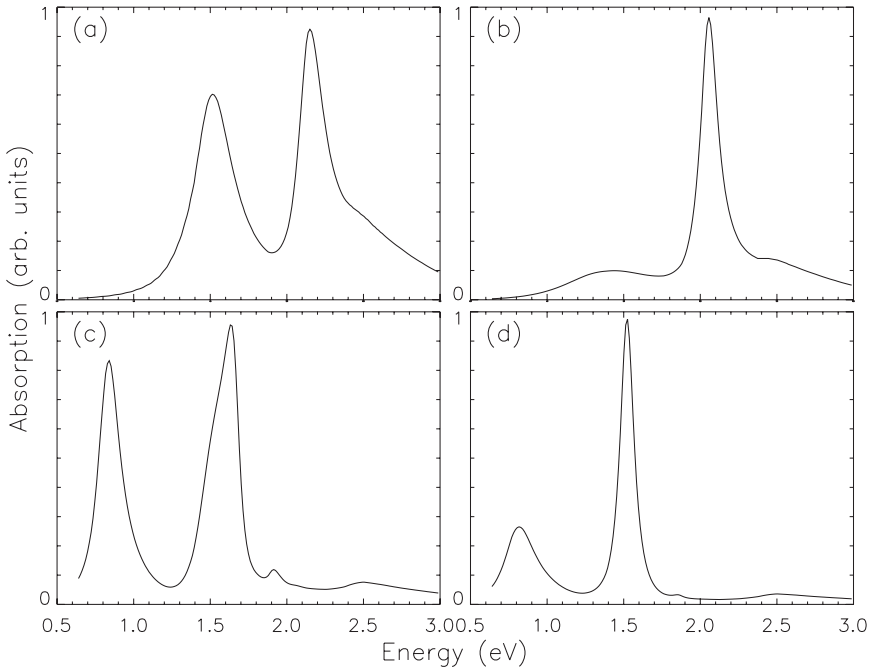

FIG. 4. Effect of the background dielectric on the optical absorption of a nanoshell near a metallic film for perpendicular polarization $m=0$. The nanoshell has $a=40$ nm, $b=50$ nm, and $Z_0=53$ nm. The film thickness is $T=8$ nm. Panel (a) shows the spectra for the film in vacuum. Panel (b) shows the spectra for $\epsilon_1=1$ and $\epsilon_2=5$. Panel (c) is for $\epsilon_1=5$ and $\epsilon_2=1$. Panel (d) is for $\epsilon_1=\epsilon_2=5$.

2.2 eV. The antibonding peak is strongly damped due to interband transitions and appears as a small shoulder around 2.5 eV. Panel (b) shows the effect when $\epsilon_2=5$ while $\epsilon_1=1$. The spectrum is similar to that in panel (a), with a small redshift of the VS as well as the localized bonding state of the nanoshell, but the intensity of the VS is reduced. This is because ϵ_2 redshifts the film continuum but does not influence the discrete nanoshell plasmon. The increased energy separation between the discrete state and the continuum reduces the magnitude of the interaction, resulting in less hybridization. Panel (c) shows the optical absorption when $\epsilon_1=5$ while $\epsilon_2=1$. Both the VS and the localized bonding nanoshell plasmon redshift significantly. The antibonding nanoshell plasmon is not affected, since it is composed primarily of cavity plasmons which do not depend on the dielectric properties of the media outside the shell. The redshift of the VS is consistent with that of both the discrete bonding nanoshell plasmon and the film plasmon continuum, redshifted by ϵ_1. The $l=2$ localized nanoshell state also appears at around 1.9 eV. Panel (d) shows the result when $\epsilon_1=\epsilon_2=5$. Compared with panel (c), we find a slight redshift of both the localized state and the VS and a strong decrease in the intensity of the VS analogous to the decrease of the VS intensity observed between panels (a) and (b). The effects of the two background dielectrics ϵ_1 or ϵ_2 can be summarized in the following manner: increasing ϵ_1 significantly redshifts both the localized state and the VS, whereas increasing ϵ_2 only weakly redshifts the localized state but reduces the intensity of the VS.

B. Finite-difference time-domain simulations

To further visualize the local electromagnetic interaction in the nanoshell and metallic film system, we have numerically calculated the extinction spectra of a nanoshell on a thin slab using the fully retarded FDTD method.[31,50,51] Our current FDTD code does not allow us to simulate a finite nanoparticle interacting with an infinite film, so the system is modeled as a nanoparticle near a finite slab. For a finite slab, the plasmons do not form a continuum, but rather, they appear as standing waves with discrete frequencies. The resulting VSs are therefore only sampled at the discrete slab plasmon energies, resulting in a VS composed of discrete slab states rather than a smooth resonance structure containing film plasmons of all wave vectors within the effective continuum. The slab we use has sufficient lateral extent that the VS is sampled in sufficient detail.[46] FDTD calculations cannot be performed efficiently for an arbitrary description of dielectric function data.[50] For this reason, in this subsection, we use a Drude fit of the Au dielectric data, $\epsilon(\omega)=\epsilon_M-\omega_B^2/\omega(\omega+i\delta)$, with $\epsilon_M=9.5$, $\omega_B=8.94$ eV, and $\delta=0.05$ eV for both the FDTD and PH calculations. This parametrization provides an accurate fit of the dielectric data for Au bulk metal above 500 nm.[31,51]

In Fig. 5, the extinction spectra from FDTD and the absorption spectra from PH are compared for nanoshells of several different aspect ratios interacting with the slab. To avoid overestimating the electromagnetic field enhancements in the junction between the particle and the film, we include a thin polyvinylpyridine (PVP) spacer layer between the nanoparticle and the film in the FDTD simulations. Such a spacer layer would need to be included in any experimental realization of a nanoparticle-film junction (and is used in the experiments and simulations on a larger nanoshell in Sec. III C). This spacer layer has no effect on the calculated extinction spectra. The size of the nanoshell is small (radius of 50 nm), so that the extinction spectra (containing both absorption and scattering terms) should be mainly determined by absorption.[52] We observe that the strengths and distribution of the discrete VS peaks calculated by FDTD fit well within the broad resonance obtained from the PH calculation, indicating good agreement between these two theoretical ap-

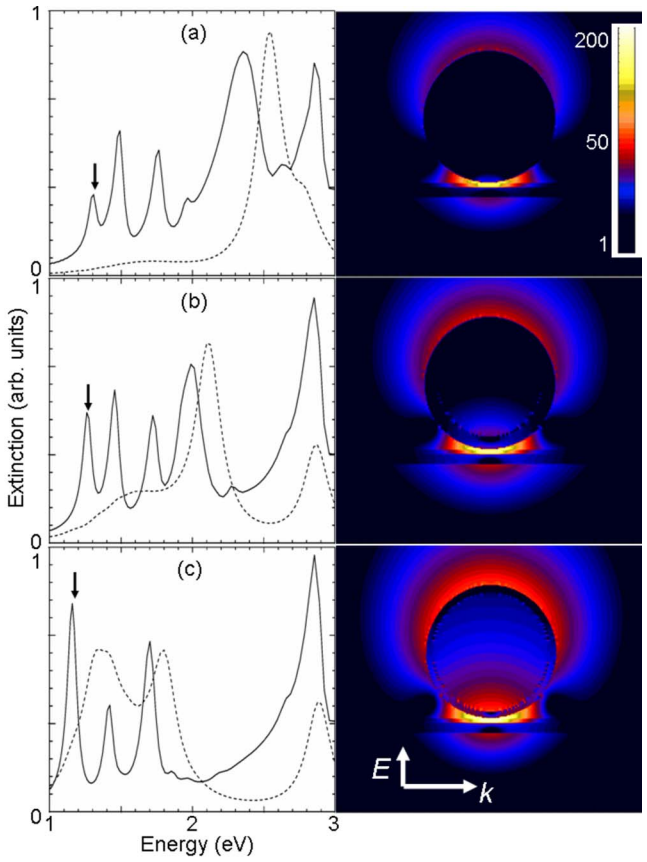

FIG. 5. (Color online) Extinction spectra (left panels) and local electric field enhancements (right panels) calculated by FDTD for the gold nanoshell/slab system for perpendicular polarization $m=0$. The slab has a thickness $T=8$ nm and lateral dimensions 300 $\times 300$ nm^2. It is covered by a PVP spacer layer ($\epsilon=2.25$) of thickness 3 nm and placed on a glass substrate ($\epsilon_2=2.25$) of thickness 100 nm. The nanoshell has an outer radius $b=50$ nm and a silica core ($\epsilon_C=2.04$). The inner radii are (a) $a=20$ nm, (b) $a=40$ nm, and (c) $a=45$ nm. The dotted lines are the absorption spectra calculated using the PH method. The arrows indicate the energies for which the electric field enhancements were calculated. The maximum field enhancement factor in each structure is 120.8, 177.2, and 244.3 for panels (a), (b), and (c), respectively.

proaches. The slight redshift of the FDTD spectra is due to retardation effects. To the right are the electric local field enhancements calculated for the specific peak labeled by the arrow in the spectra. Enhancement is defined here as the absolute value of the electromagnetic field at a specific point divided by the absolute value of the incident field. For simplicity, we show the enhancement only for the lowest-energy discrete peak in the VS.[46] The calculated electric field enhancements are large and show that the VS represents a strong coupling between the nanoshell and the film. As the aspect ratio of the nanoshell increases, the electric field enhancement increases from 121 to 244. Compared to the field enhancement factors obtained previously for the nanosphere/film system,[46] we find that the thin nanoshell and film interaction produces a VS of lower energy and larger local field enhancements. This shows that the nanoshell/film system is a more suitable substrate for surface enhanced spectroscopy studies than the nanosphere/film structure.

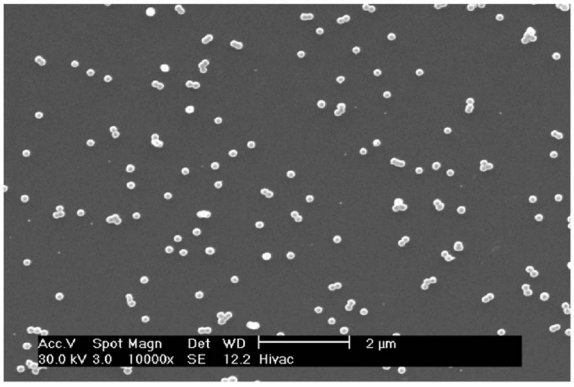

FIG. 6. SEM image of a representative sample of a thin Au layer on which Au nanoshells have been dispersed. The Au film thickness is 4 nm and the nanoshell has a 60 nm radius core made from SiO_2 and a shell thickness of 10 nm. The Au film is thermally evaporated onto a clean glass slide at base pressure of 10^{-6} torr. A thin Ti film with 1.5 nm thickness is used as an adhesion layer between the gold film and the glass substrate. A spacer layer of (3.5 ± 0.5) nm is formed by depositing polyvinylpyridine (PVP) from a 1% ethanol solution for 8 h.

The electric field enhancements for excitation of the $m=1$ VS (not shown) are much smaller than those for $m=0$. The magnitude is similar to the enhancements of an individual nanoshell but the location is in the junction between the nanoshell and the film.

C. Experimental measurements

In this section, we show experimental results for the extinction spectra of the nanoshell/film system. The fabrication details are similar to those reported in our previous study of the nanosphere/film structure.[43] In Fig. 6, a scanning electron microscopy (SEM) image of a representative sample is shown. This image shows that the number density of nanoshells over the film is low. The majority of nanoshells scatter sparsely onto the film but many form aggregates and are therefore also sampled in the experiment. The theoretical calculations presented in this section refer to the highly idealized situation of an isolated nanoshell on a uniform thin film. We do not try to model local variations of film thickness, nonuniform nanoshell-film separations, or the effect of nanoshell-nanoshell interactions. Instead, we focus more on trends such as the effect of polarization, film thickness, and dielectric overlayers rather than attempting a quantitative explanation of experimental data. The incident laser beam comes from beneath the film and the extinction spectra are determined by subtracting the transmitted light from the incident light. The incidence angle is defined as the angle between the wave vector of the incident light and the surface normal of the film.

Extinction spectra for each sample were taken using *p*-polarized light with the incident angle varied from 0° to 80° at 10° intervals. In Fig. 7, the raw extinction spectra are shown for one of the samples of nanoshell/metallic film

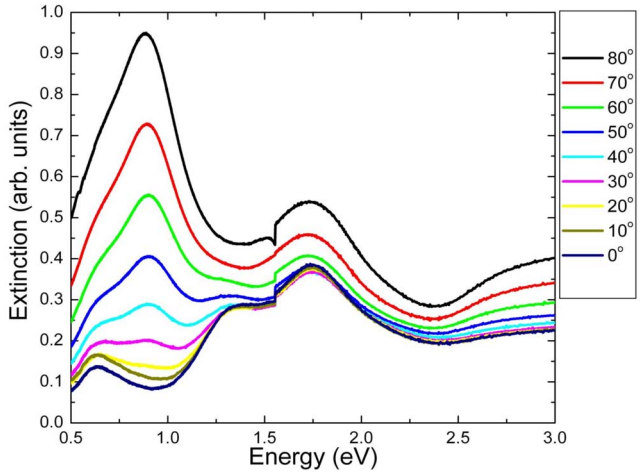

FIG. 7. (Color online) Experimental extinction spectra of the nanoshell/film system with film thickness of 12 nm. The spectra are taken using p-polarized light at varying incident angles.

structures as a function of incident angle. The Au film thickness is 12 nm. An incidence angle of 0° refers to light polarized parallel to the surface (normal incidence) that can interact with $m=1$ plasmons. Varying the angle from normal incidence in TM, or p polarization, the largest angle of incidence that can be achieved in the experiment is 80°. This near grazing incidence angle results in light polarized 96% ($\sin^2 80°$) perpendicular and 4% ($\cos^2 80°$) parallel to the film. We refer to this geometry as perpendicular polarization; it predominantly couples to $m=0$ plasmons although a small fraction of $m=1$ modes are excited at this angle.

At normal incidence (0°), the spectrum is characterized by two peaks, a peak at 1.8 eV and a broad shoulder around 1.3 eV. These features correspond to the localized state above the continuum and an $m=1$ VS in the continuum, respectively. As the angle is increased, the $m=1$ VS remains at 1.3 eV but its intensity is quickly overwhelmed by the appearance of a new feature at around 0.8 eV. This feature is the $m=0$ VS. The energy of the localized state at 1.8 eV does not depend on polarization, since it is essentially composed of a pure bonding nanoshell dipolar plasmon.[46] The discontinuity around 1.6 eV is an experimental artifact caused by a change of spectrometer grating at 800 nm. (In the following spectra, this discontinuity is removed by a linear interpolation procedure.) The nature of the weak feature around 0.65 eV which appears most clearly at normal incidence is unknown. Possible origins include a nanoshell dimer or aggregate resonance which for normal incidence would be redshifted to below 1 eV or a Fabry-Pérot resonance generated by the glass substrate.

In order to experimentally investigate the effect of the dielectric embedding medium surrounding the nanoshell (ϵ_1) on the extinction spectra, a thick layer (nominally 10 μm) of PVP, fully embedding the layer of dispersed nanoshells, was spin coated onto the substrates. In the following, we will refer to the samples where PVP is present only as a spacer layer between the film and the nanoshell as air-ambient samples.

In Fig. 8, the extinction spectra for perpendicular polarization ($m=0$) for air-ambient and PVP-coated samples are shown. Each measurement is performed for four different film thicknesses, $T=4,8,12,16$ nm, respectively. For the air-ambient samples [panel (a)], the peak around 1.7 eV is the localized bonding nanoshell dipolar resonance, which is independent of film thickness. The VS shifts to lower energies from around 0.9 eV for $T=16$ nm to nominally 0.7 eV for $T=4$ nm. Panel (b) shows the effects of the PVP overcoating. Both the localized state and the VS are redshifted compared to the air-ambient samples. The localized state appears at an energy around 1.5 eV, and the VS redshifts from around 0.75 eV for $T=16$ nm to 0.54 eV for $T=4$ nm. The peak intensities in the PVP-coated samples are strongly sup-

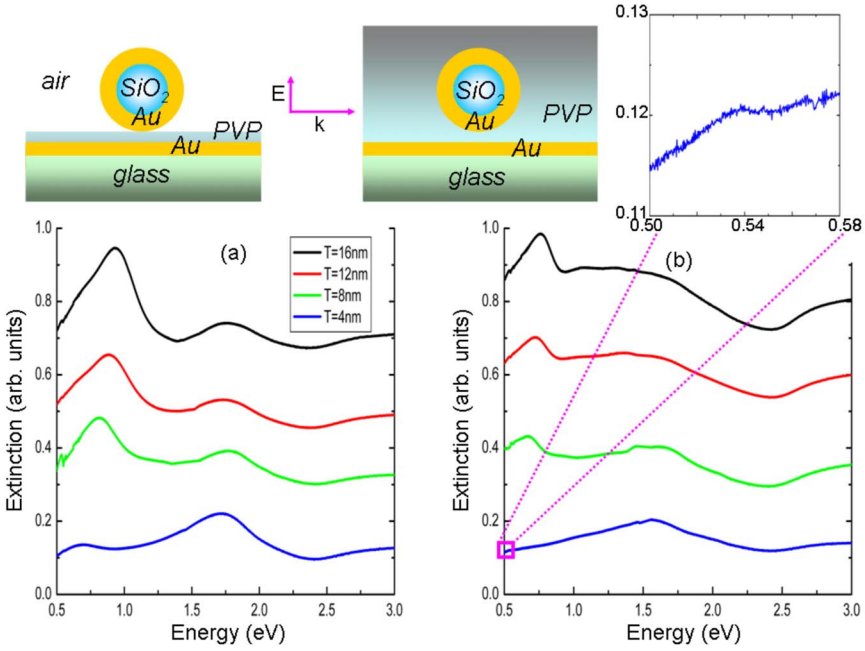

FIG. 8. (Color online) Extinction spectra for perpendicular polarization $m=0$ measured for (a) air-ambient and (b) PVP-coated samples. In each panel, the measurement is performed for four different film thicknesses, $T=4,8,12,16$ nm, respectively. The inset in panel (b) is the magnified low-energy part of the $T=4$ nm curve for identifying the VS.

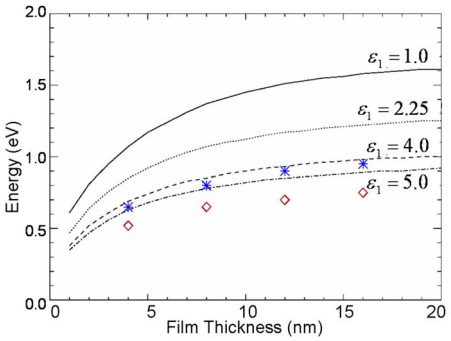

FIG. 9. (Color online) Comparison of experimentally obtained energies of the $m=0$ VS with the results from PH as a function of film thickness for different dielectric constants of the embedding medium ϵ_1. The curves are the theoretical calculations with ϵ_1 increasing from 1.0 to 5.0. The blue and red symbols are the experimental measurements for air-ambient and PVP-overcoated samples, respectively.

pressed relative to the air-ambient samples due to the dielectric screening. In the inset of panel (b), we show a close-up of the low-energy part of the $T=4$ nm curve where the VS appears as a shoulder around 0.54 eV.

In Fig. 9, we compare the energy of the VS determined from the experimental spectra with those obtained from PH as a function of film thicknesses for different surrounding media ϵ_1. The important trend of a decreasing energy of the VS with reduced film thickness is reproduced very well. The best fit is obtained for $\epsilon_1=4$, which is larger than the experimental value of $\epsilon_1=2.25$ for bulk PVP. Possible reasons for the discrepancy may be local variations of the dielectric environment of the nanostructures or the neglect of retardation effects, which for the present system of a nanoshell of radius 70 nm can be as large as 0.15 eV (estimated from the Mie theory for a spherical nanoshell).

In Fig. 10, the energy of the $m=1$ VS obtained from the measurements is compared to the results from the PH method. As for the $m=0$ polarization, the energy of the VS state shifts to lower energies with decreasing film thickness. Interestingly, though the overall interaction energy for the

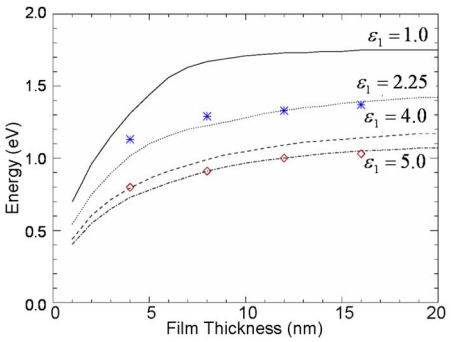

FIG. 10. (Color online) Comparison of experimentally obtained energies of the $m=1$ VS with the results from PH as a function of film thickness for different dielectric constants of the embedding medium ϵ_1. The lines and the symbols refer to the same structures as in Fig. 9.

$m=1$ polarization is weaker than that for the $m=0$ polarization, we find that the effect of overcoating with PVP is much larger for the $m=1$ polarization than for the $m=0$ polarization. The reason is that the energy of the virtual state depends on the difference in energy between the discrete nanoshell state and the effective continuum.

On the air-ambient sample for the $m=0$ polarization, the surface charges associated with the discrete nanoshell plasmon are located in the junction between the nanoparticle and the film and on top of the nanoshell. The PVP spacer layer thus screens both the nanoshell mode and the bare thin film plasmons. This screening results in a redshift of both the nanoshell mode and the effective film continuum which enables a more efficient interaction as discussed in Fig. 4. For the $m=1$ polarization, where the effective dipole lies parallel to the film, the effect of the PVP coating is different. On the air-ambient sample, only the film plasmons are screened, since the surface charges associated with the discrete nanoshell plasmon are located at a distance b from the spacer layer. The effect of PVP coating is an efficient screening and a redshifting of the discrete nanoshell plasmon mode. The redshift brings the mode closer to the effective film continuum, resulting in a stronger redshift of the VS.

IV. DISCUSSION AND CONCLUSIONS

In this paper, we have shown that the metallic nanoshell/film system represents a highly tunable plasmonic structure with strong resonances in the infrared region of the spectrum, accompanied by large local electric field enhancements. This easily fabricated geometry has properties that are of fundamental physical interest, as an experimental physics test bed where the parameters of the spinless Anderson model can be varied controllably. The "antenna-overconducting-plane" paradigm for this system lends it naturally to a variety of applications in subwavelength plasmon optics. This geometry provides a wavelength-specific method for the selective coupling of light to or from freely propagating light waves and surface plasmons, of likely importance for plasmon-based devices. The large local fields in the particle-film junction provide an important model for tip-sample junctions in scanning microscopies such as near-field scanning optical microscopy, enabling the design of both tip and substrate for scanning tip-enhanced Raman spectroscopy. In our theoretical analysis of this system, we have shown how the plasmon hybridization method can be extended to include electrostatic screening from background dielectrics. We have shown that in the limit of a thin metallic film, the interaction between the discrete nanoshell plasmons and the continuum of delocalized film plasmons can result in a low-energy virtual state. The electromagnetic field enhancements induced by excitation of the virtual states are of similar magnitude to those obtained in the junction of a nanoparticle dimer. The energy of the virtual state can be tuned by changing the aspect ratio of the nanoshell and/or by changing the thickness of the film. Further studies including the application of periodic boundary FDTD for modeling a continuous film, and thus the VS, more accurately and single particle optical measurements are currently in progress.

ACKNOWLEDGMENTS

This material is based on work supported by the U.S. Army Research Laboratory and the U.S. Army Research Office under Grant No. W911NF-04-1-0203, the Robert A. Welch Foundation under Grants Nos. C-1220 and C-1222, and NSF under Grants Nos. EEC-0304097 and ECS-0421108.

APPENDIX A: DERIVATION OF THE LAGRANGIAN

The primitive film plasmons can be expressed in cylindrical Bessel functions with an origin centered on the projection of the center of nanoshell on the film. $\vec{\rho}=(\rho,\phi)$ denotes the lateral position along the surface and z is the coordinate perpendicular to the surface. For the nanoshell plasmons, we use spherical coordinates.

The Lagrangian for the nanoshell plasmons has been previously derived,[47] in which we showed that the plasmon energies of a nanoshell depend on $\omega_{B,S}=\sqrt{\frac{4\pi e^2 n_S}{m_e}}$, multipolar index l, and its aspect ratio $x=a/b$,

$$\omega_{\pm}^2(x)=\frac{\omega_{B,S}^2}{2}\left[1\pm\frac{1}{2l+1}\sqrt{1+4l(l+1)x^{2l+1}}\right]. \quad \text{(A1)}$$

The bonding $(-)$ and antibonding $(+)$ eigenmodes are related to the primitive cavity and sphere modes as

$$N_{lm}^{+}=C_{lm}\sin\xi_l-S_{lm}\cos\xi_l,$$

$$N_{lm}^{-}=C_{lm}\cos\xi_l+S_{lm}\sin\xi_l, \quad \text{(A2)}$$

where $\tan\xi_l=\frac{\omega_{C,l}\omega_{S,l}}{\omega_{l+}^2-\omega_{C,l}^2}x^{l+1/2}$.

The kinetic energy of the primitive plasmons of the film can be expressed as

$$T^{film}=\frac{n_F m_e}{2}\int dS\,\eta^*\nabla\,\eta, \quad \text{(A3)}$$

where the integral is over the two surfaces of the film and the $*$ superscript denotes the complex conjugate. The integral can be evaluated analytically:

$$T^{film}=\frac{n_F m_e}{2}\int\frac{d\vec{k}}{(2\pi)^2}k(1-e^{-2kT})[\dot{P}_{\vec{k}}^2+\dot{Q}_{\vec{k}}^2]. \quad \text{(A4)}$$

The potential energy of the primitive plasmons of the film can be expressed as

$$V^{film}=\frac{1}{2}\int dS\phi^*\sigma, \quad \text{(A5)}$$

where $\phi(\vec{r})$ and $\sigma(\vec{r})$ are the electrostatic potential and surface charge generated by the primitive plasmons of the film, respectively. The integral can be evaluated analytically and takes the form

$$V^{film}=\frac{n_F m_e}{2}\frac{\omega_{B,F}^2}{2}\int\frac{d\vec{k}}{(2\pi)^2}k(1-e^{-2kT})\times[P_{\vec{k}}^2+Q_{\vec{k}}^2-2P_{\vec{k}}Q_{\vec{k}}e^{-kT}]. \quad \text{(A6)}$$

The Lagrangian for the film $L^{film}=T^{film}-V^{film}$ can be written in a diagonal form by introducing bonding and antibonding combinations of P and Q,

$$M_{\vec{k}\pm}=\frac{1}{\sqrt{2}}(P_{\vec{k}}\pm Q_{\vec{k}}), \quad \text{(A7)}$$

which can be shown to correspond to the plasmonic states of a thin film with energies

$$\omega_{\vec{k},\pm}(T)=\frac{\omega_{B,F}}{\sqrt{2}}\sqrt{1\pm\exp[-kT]}. \quad \text{(A8)}$$

In this representation, the Lagrangian takes the form

$$L^{film}=\frac{n_F m_e}{2}\sum_{j=\pm}\int\frac{d\vec{k}}{(2\pi)^2}k(1-e^{-2kT})[\dot{M}_{\vec{k}j}^2-\omega_{\vec{k}j}^2M_{\vec{k}j}^2]. \quad \text{(A9)}$$

The surface plasmons of the film form a continuous band ranging from zero energy up to the bulk plasmon frequency of the metal. The plasmonic density of states is peaked around the surface plasmon energy $\omega_{sp}=\omega_{B,F}/\sqrt{2}$. The plasmonic density of states depends strongly on film thickness. For infinite thickness, the film plasmons have no dispersion and the plasmonic density of states is a delta function centered on the surface plasmon energy $\omega_{sp}=\omega_{B,F}/\sqrt{2}$. For decreasing film thickness, the density of states broadens in energy. The modes $M_{\vec{k}\pm}$ represent the linearly independent, noninteracting plasmons of a thin film. In the presence of the nanoparticle, they no longer represent stationary states of the system.

The interaction between the film plasmons and the nanoshell plasmons is conveniently evaluated as an integral over the surface charge of the shell and takes the form

$$V=\sum_{lm}\int\frac{d\vec{k}}{(2\pi)^2}R^2\int d\Omega_{C,S}\phi_{\vec{k}i}^*(\vec{r})\sigma_{lm}(\Omega_{C,S}), \quad \text{(A10)}$$

where

$$\phi_{\vec{k}i}=\sqrt{2}\pi n_F e M_{\vec{k}i}(1-e^{-2kT})e^{i\vec{k}\cdot\vec{\rho}}e^{-kz} \quad \text{(A11)}$$

is the electrostatic potential outside the film (for $z>0$) from the primitive film plasmons and σ_{lm} is the charge density associated with the shell plasmons on both the cavity and the outer sphere surfaces.

We now make use of the azimuthal symmetry of the problem and expand the exponential terms in $\phi_{\vec{k}i}$ in a Fourier series[37]

$$e^{i\vec{k}\cdot\vec{\rho}}=\sum_m i^m e^{-im\phi'}J_m(k\rho)e^{im\phi}, \quad \text{(A12)}$$

where J_m is a cylindrical Bessel function of order m. We also introduce the Fourier transform

$$M_j(k,m)=\frac{i^m}{\sqrt{2\pi}}\int d\phi' M_{\vec{k}j}\exp[-im\phi']. \quad \text{(A13)}$$

In this notation, the interaction V becomes diagonal in azimuthal m and the Lagrangian of the combined system can be written as $L=\Sigma_m L^m$, where

$$L^m = \frac{n_S m_e}{2}\sum_{l,i=\pm}[\dot{N}^2_{lm,i} - \omega^2_{l,i}N^2_{lm,i}] + \frac{n_F m_e}{2}\sum_{j=\pm}\int \frac{dk}{(2\pi)^2}k^2(1 - e^{-2kT})[\dot{M}^2_j(k,m) - \omega^2_{k,j}M^2_j(k,m)] + \sqrt{\pi}n_F n_S e^2 \sum_l \sqrt{lR}y^m_l \sum_{i=\pm,j=\pm}\int dkk(1 - e^{-2kT})e^{-kZ_0}I^m_{lk,i,j}N_{lm,i}M_j(k,m), \quad \text{(A14)}$$

where Z_0 is the distance between the center of the shell and the film surface and y^m_l is the normalization constant for the spherical harmonics. The integrals are

$$I^m_{kl,+,+} = I^m_{kl,+,-} = F_1 I^m_{Ckl} + F_3 I^m_{Skl},$$

$$I^m_{kl,-,+} = I^m_{kl,-,-} = F_2 I^m_{Ckl} + F_4 I^m_{Skl}, \quad \text{(A15)}$$

where

$$I^m_{Ckl} = \int_0^\pi d\theta \sin\theta J_m(ka\sin\theta)P^m_l(\cos\theta)e^{-ka\cos\theta} = \frac{2}{2l+1}\frac{(-ka)^l}{(l-m)!},$$

$$I^m_{Skl} = \int_0^\pi d\theta \sin\theta J_m(kb\sin\theta)P^m_l(\cos\theta)e^{-kb\cos\theta} = \frac{2}{2l+1}\frac{(-kb)^l}{(l-m)!}, \quad \text{(A16)}$$

and

$$F_1 = \sqrt{\frac{l+1}{a^3}}\sin\xi_l + x^{l-1}\sqrt{\frac{l}{b^3}}\cos\xi_l,$$

$$F_2 = \sqrt{\frac{l+1}{a^3}}\cos\xi_l - x^{l-1}\sqrt{\frac{l}{b^3}}\sin\xi_l,$$

$$F_3 = -x^{l+2}\sqrt{\frac{l+1}{a^3}}\sin\xi_l - \sqrt{\frac{l}{b^3}}\cos\xi_l,$$

$$F_4 = -x^{l+2}\sqrt{\frac{l+1}{a^3}}\cos\xi_l + \sqrt{\frac{l}{b^3}}\sin\xi_l. \quad \text{(A17)}$$

With the substitutions

$$N_{lm,i} \to \sqrt{\frac{2}{n_S m_e}}N_{lm,i} \quad \text{(A18)}$$

and

$$M_j(k,m) \to \frac{2\pi}{k\sqrt{1-e^{-2kT}}}\sqrt{\frac{2}{n_F m_e}}M_j(k,m), \quad \text{(A19)}$$

the interaction term takes the form

$$V^m_{lk,i,j}(Z_0) = \sqrt{\pi}\omega_{B,F}\omega_{B,S}y^m_l\sqrt{lR}\sqrt{1-e^{-2kT}}e^{-kZ_0}I^m_{lk,i,j}, \quad \text{(A20)}$$

resulting in the Lagrangian in Eq. (2).

APPENDIX B: DISCRETIZATION AND VECTOR NOTATION

The Lagrangian in Eq. (2) can be discretized by introducing a vector $\vec{X}$ representing the amplitudes of the primitive plasmons. A particularly convenient choice is

$$\vec{X} = (N^-_{lm}, N^+_{lm}; \sqrt{\Delta k}M_-(k,m), \sqrt{\Delta k}M_+(k,m))^T, \quad \text{(B1)}$$

with $l=1,2,\ldots,l_{max}$ and $k=1,2,\ldots,k_{max}$. In this expression, Δk is the spacing between adjacent wave vectors of the thin film plasmons.

In this representation, the kinetic energy matrix $\hat{T}_X$ is diagonal with

$$\hat{T}_X = \begin{pmatrix} 1-x^{2l+1} & & 0 \\ & \cdots & \\ 0 & & 1-e^{-2kT} \end{pmatrix}, \quad \text{(B2)}$$

with $l=1,2,\ldots,l_{max}$ and $k=1,2,\ldots,k_{max}$.

The potential energy matrix takes the form

$$\hat{V}_X = \begin{pmatrix} \hat{V}_{ll} & \hat{V}_{lk} \\ \hat{V}_{kl} & \hat{V}_{kk} \end{pmatrix}, \quad \text{(B3)}$$

where $l=1,2,\ldots,l_{max}$ and $k=1,2,\ldots,k_{max}$, with

$$\hat{V}_{ll} = (1-x^{2l+1})\begin{pmatrix} \omega^2_{l,-}(x) & 0 \\ 0 & \omega^2_{l,+}(x) \end{pmatrix}, \quad \text{(B4)}$$

$$\hat{V}_{kk} = (1-e^{-2kT})\begin{pmatrix} \omega^2_{k,-}(T) & 0 \\ 0 & \omega^2_{k,+}(T) \end{pmatrix}, \quad \text{(B5)}$$

and

$$\hat{V}_{lk} = \hat{V}_{kl} = \frac{1}{2}y^m_l\sqrt{\pi\Delta k}\omega_{B,S}\omega_{B,F}(1-e^{-2kT})e^{-kZ_0}\begin{pmatrix} I^m_{kl,-,-} & I^m_{kl,-,+} \\ I^m_{kl,+,-} & I^m_{kl,+,+} \end{pmatrix}. \quad \text{(B6)}$$

The appearance of the $\sqrt{\Delta k}$ term here and in several equations below is due to our choice of $\vec{X}$ in Eq. (B1).

It is useful to introduce a vector $\vec{\sigma}$ representing the surface charges associated with the primitive plasmons. We define this vector as

$$\vec{\sigma} = (\sigma_{C,l}, \sigma_{S,l}, \Delta k\sigma_{P,k}, \Delta k\sigma_{Q,k})^T, \quad \text{(B7)}$$

where $l=1,2,\ldots,l_{max}$, $k=1,2,\ldots,k_{max}$. The surface charges $\sigma_{C,l}$ and $\sigma_{S,l}$ are the surface charges associated with the discrete cavity and sphere plasmons of the nanoshell and $\sigma_{P,k}$ and $\sigma_{Q,k}$ are the surface charges associated with the primitive film plasmons for a specific wave vector k. The Δk factor in front of the primitive film plasmons arises from our discrete sampling of a continuum of primitive film plasmons.

With this definition, the physical surface charges associated with the primitive plasmons can be expressed as $\vec{\sigma} = \hat{B} \cdot \hat{X}$, where

$$\hat{B} = \begin{pmatrix} \hat{B}_{shell} & 0 \\ 0 & \hat{B}_{film} \end{pmatrix}. \tag{B8}$$

The transformation matrix for the nanoshell takes the form

$$\hat{B}_{shell} = n_s e \begin{pmatrix} \hat{B}_1 & & 0 \\ & \cdots & \\ 0 & & \hat{B}_{l_{max}} \end{pmatrix}, \tag{B9}$$

with

$$\hat{B}_l = \begin{pmatrix} F_2 & F_1 \\ F_4 & F_3 \end{pmatrix}, \tag{B10}$$

where the quantities F_i are defined in Eq. (A17). The transformation matrix for the film takes the form

$$\hat{B}_{film} = n_f e \begin{pmatrix} \hat{B}_1 & & 0 \\ & \cdots & \\ 0 & & \hat{B}_{k_{max}} \end{pmatrix}, \tag{B11}$$

with

$$\hat{B}_k = \sqrt{\Delta k} \begin{pmatrix} 1 + e^{-kT} & 1 - e^{-kT} \\ -1 - e^{-kT} & 1 - e^{-kT} \end{pmatrix}. \tag{B12}$$

In the discussion of the effects of background dielectrics, it becomes useful to express the potential energy of the system in terms of the surface charge vector $\vec{\sigma}$,

$$V = \frac{1}{2} \vec{\sigma}^T \hat{V}_\sigma \vec{\sigma}. \tag{B13}$$

In this representation, the potential energy matrix takes the form

$$\hat{V}_\sigma = (\hat{B}^{-1})^T \hat{V}_X \hat{B}^{-1}. \tag{B14}$$

To achieve convergence for the systems studied in the present paper, we include all nanoshell plasmons up to $l_{max} = 40$ and employ a uniform discretization of the film continuum with a wave vector cutoff of 1 nm^{-1} and $k_{max} = 800$.

APPENDIX C: EFFECTS OF DIELECTRIC BACKGROUND

In this section, we discuss the effects of dielectric screening in the structure. We consider background dielectric polarizabilities of the metallic structures and the dielectrics of nonplasmonic embedding media. We will use the following notations to represent the permittivities of the different media: ϵ_C for the nanoshell core, ϵ_S for the metallic shell, ϵ_1 for an embedding medium around the nanoshell and above the metallic film, ϵ_F for metallic film background, and ϵ_2 for a dielectric substrate below the metallic film.

The effects of background dielectrics in the PH method are straightforward. In the presence of background dielectrics, the electrostatic energy in the system takes the form

$$V = \frac{1}{2} \vec{\sigma}^T \hat{V}_\sigma \vec{\sigma}^{total}, \tag{C1}$$

where σ refers to the real surface charge densities induced by the primitive plasmons and σ^{total} are the total surface charges (real+induced). The effects of background dielectric can thus be conveniently included through a matrix $\hat{\chi}$ that relates the total charges to the real charges, $\vec{\sigma}^{total} = \hat{\chi} \vec{\sigma}$. Using this relation, the potential energy for the primitive plasmons in the presence of dielectric backgrounds takes the form

$$V = \frac{1}{2} \vec{\sigma}^T \hat{V}_\sigma \hat{\chi} \vec{\sigma} = \frac{1}{2} \vec{X}^T \hat{V}_X \hat{B}^{-1} \hat{\chi} \hat{B} \vec{X} = \frac{1}{2} \vec{X}^T \hat{V}_X^D \vec{X}, \tag{C2}$$

where $\hat{V}_X^D = \hat{V}_X \hat{B}^{-1} \hat{\chi} \hat{B}$ is the potential energy matrix for dielectric systems and $\hat{V}_X$ is the potential energy matrix calculated in the absence of dielectric backgrounds.

The inverse matrix $\hat{E} = \hat{\chi}^{-1}$ can be calculated directly from the discontinuities of the displacement field at the boundaries of the dielectrics,

$$\epsilon_{i+1} \left. \frac{\partial \Phi}{\partial r} \right|_{R_i^+} - \epsilon_i \left. \frac{\partial \Phi}{\partial r} \right|_{R_i^-} = -4\pi\sigma_i, \tag{C3}$$

where Φ_i is the potential generated by the ith total surface charge.

The electrostatic potential from the primitive plasmons of the nanoshell takes the form

$$\Phi_{shell} = \sum_l \frac{4\pi}{2l+1} [a^2 v_l(r,a) \sigma_{C,l}^{total} + b^2 v_l(r,b) \sigma_{S,l}^{total}], \tag{C4}$$

with $v_l(r,r') = \frac{r_<^l}{r_>^{l+1}}$, where $r_<$ and $r_>$ refer to the smaller and the larger of r and r', respectively. The electrostatic potential from the primitive film plasmons takes the form

$$\Phi_{film} = \sum_k \frac{2\pi}{k} [e^{-k|z|} \sigma_{P,k}^{total} + e^{-k|z+T|} \sigma_{Q,k}^{total}]. \tag{C5}$$

Using these two expressions, the final expression for the matrix $\hat{E}$ is

$$\hat{E} = \begin{pmatrix} \hat{E}_{ll} & \hat{E}_{lk} \\ \hat{E}_{kl} & \hat{E}_{kk} \end{pmatrix}, \tag{C6}$$

where $l = 1, 2, \ldots, l_{max}$ and $k = 1, 2, \ldots, k_{max}$, with

$$\hat{E}_{ll} = \begin{pmatrix} \frac{\epsilon_S(l+1) + \epsilon_C l}{2l+1} & \frac{(\epsilon_C - \epsilon_S) l x^{l-1}}{2l+1} \\ \frac{(\epsilon_1 - \epsilon_S)(l+1) x^{l+2}}{2l+1} & \frac{\epsilon_1(l+1) + \epsilon_S l}{2l+1} \end{pmatrix}, \tag{C7}$$

$$\hat{E}_{kk} = \begin{pmatrix} \frac{\epsilon_1 + \epsilon_F}{2} & \frac{\epsilon_1 - \epsilon_F}{2} e^{-kT} \\ \frac{\epsilon_2 - \epsilon_F}{2} e^{-kT} & \frac{\epsilon_F + \epsilon_2}{2} \end{pmatrix}, \tag{C8}$$

$$\hat{E}_{lk} = \sqrt{\frac{\pi}{2k}} y_l^m l e^{-kZ_0} \begin{pmatrix} (\epsilon_C - \epsilon_S)\frac{I_{Ckl}^m}{a} & (\epsilon_C - \epsilon_S)\frac{I_{Ckl}^m}{a} e^{-kT} \\ (\epsilon_S - \epsilon_1)\frac{I_{Skl}^m}{b} & (\epsilon_S - \epsilon_1)\frac{I_{Skl}^m}{b} e^{-kT} \end{pmatrix}, \tag{C9}$$

and

$$\hat{E}_{kl} = -\sqrt{\frac{\pi}{2}} y_l^m lk\Delta k e^{-kZ_0} \times \begin{pmatrix} (\epsilon_1 - \epsilon_F) I_{Ckl}^m a^2 & (\epsilon_1 - \epsilon_F) I_{Skl}^m b^2 \\ (\epsilon_F - \epsilon_2) I_{Ckl}^m a^2 e^{-kT} & (\epsilon_F - \epsilon_2) I_{Skl}^m b^2 e^{-kT} \end{pmatrix}. \tag{C10}$$

*Corresponding author. FAX: (713)348-4150; nordland@rice.edu

[1] R. Jin, Y. Wei, C. A. Mirkin, K. L. Kelly, G. C. Schatz, and J. G. Zheng, Science **294**, 1901 (2001).

[2] W. L. Barnes, A. Dereux, and T. W. Ebbeson, Nature (London) **424**, 824 (2003).

[3] S. I. Bozhevolnyi, E. D. V. S. Volkov, J. Y. Laluet, and T. W. Ebbeson, Nature (London) **440**, 508 (2006).

[4] S. Nie and S. R. Emory, Science **275**, 1102 (1997).

[5] K. Kneipp, Y. Wang, H. Kneipp, L. T. Perelman, I. Itzkan, R. R. Dasari, and M. S. Feld, Phys. Rev. Lett. **78**, 1667 (1997).

[6] A. M. Michaels, M. Nirmal, and L. E. Brus, J. Am. Chem. Soc. **121**, 9932 (1999).

[7] H. Xu, E. J. Bjerneld, M. Kall, and L. Borjesson, Phys. Rev. Lett. **83**, 4357 (1999).

[8] G. C. Schatz and R. P. van Duyne, in *Handbook of Vibrational Spectroscopy*, edited by J. M. Chalmers and P. R. Griffiths (Wiley, Chichester, 2002), pp. 1–16.

[9] M. Moskovits and D. H. Jeong, Chem. Phys. Lett. **397**, 91 (2004).

[10] J. B. Jackson and N. J. Halas, Proc. Natl. Acad. Sci. U.S.A. **101**, 17930 (2004).

[11] S. A. Maier, P. E. Barclay, T. J. Johnson, M. D. Friedman, and O. Painter, Appl. Phys. Lett. **84**, 3990 (2004).

[12] S. A. Maier, M. L. Brongersma, P. G. Kik, S. Meltzer, A. G. Requicha, and H. A. Atwater, Adv. Mater. (Weinheim, Ger.) **13**, 1501 (2001).

[13] M. Quinten, A. Leitner, J. R. Krenn, and F. R. Aussenegg, Opt. Lett. **23**, 1331 (1998).

[14] J. Takahara, S. Yamagishi, H. Taki, A. Morimoto, and T. Kobayashi, Opt. Lett. **22**, 475 (1997).

[15] J. R. Krenn, B. Lamprecht, H. Ditlbacher, G. Schider, M. Salerno, A. Leitner, and F. R. Aussenegg, Europhys. Lett. **60**, 663 (2002).

[16] R. Zia, M. D. Selker, P. B. Catrysse, and M. L. Brongersma, J. Opt. Soc. Am. A **21**, 2442 (2004).

[17] S. Oldenburg, R. D. Averitt, S. Westcott, and N. J. Halas, Chem. Phys. Lett. **288**, 243 (1998).

[18] S. Link and M. A. El-Sayed, J. Phys. Chem. B **103**, 8410 (1999).

[19] T. R. Jensen, M. D. Malinsky, C. L. Haynes, and R. P. van Duyne, J. Phys. Chem. B **104**, 10549 (2000).

[20] J. Aizpurua, P. Hanarp, D. S. Sutherland, M. Kall, G. W. Bryant, and F. J. Garcia de Abajo, Phys. Rev. Lett. **90**, 057401 (2003).

[21] A. Dmitriev, T. Pakizeh, M. Kall, and D. S. Sutherland, Small **3**, 294 (2007).

[22] C. J. Murphy, T. K. San, C. J. Orendorff, J. X. Gao, L. Gou, S. E. Hunyadi, and T. Li, J. Phys. Chem. B **109**, 13857 (2005).

[23] Z. Yuan and S. Gao, Phys. Rev. B **73**, 155411 (2006).

[24] B.-H. Choi, H.-H. Lee, S. Jin, S. Chun, and S.-H. Kim, Nanotechnology **18**, 075706 (2007).

[25] F. Wang and Y. R. Shen, Phys. Rev. Lett. **97**, 206806 (2006).

[26] P. K. Aravind, A. Nitzan, and H. Metiu, Surf. Sci. **110**, 189 (1981).

[27] K. Li, M. I. Stockman, and D. J. Bergman, Phys. Rev. Lett. **91**, 227402 (2003).

[28] K. H. Su, Q. H. Wei, X. Zhang, J. J. Mock, D. R. Smith, and S. Schultz, Nano Lett. **3**, 1087 (2003).

[29] W. Rechberger, A. Hohenau, A. Leitner, J. R. Krenn, B. Lamprecht, and F. R. Aussenegg, Opt. Commun. **220**, 137 (2003).

[30] D. P. Fromm, A. Sundaramurthy, P. J. Schuck, G. Kino, and W. E. Moerner, Nano Lett. **5**, 957 (2005).

[31] C. Oubre and P. Nordlander, J. Phys. Chem. B **109**, 10042 (2005).

[32] C. Dahmen, B. Schmidt, and G. von Plessen, Nano Lett. **7**, 318 (2007).

[33] P. Aravind and H. Metiu, Surf. Sci. **124**, 506 (1983).

[34] R. Ruppin, Phys. Rev. B **45**, 11209 (1992).

[35] V. V. Gozhenko, L. G. Grechko, and K. W. Whites, Phys. Rev. B **68**, 125422 (2003).

[36] M. Futamata, Y. Maruyama, and M. Ishikawa, J. Phys. Chem. B **107**, 7607 (2003).

[37] P. Nordlander and E. Prodan, Nano Lett. **4**, 2209 (2004).

[38] S. A. Maier, M. L. Brongersma, P. G. Kik, and H. A. Atwater, Phys. Rev. B **65**, 193408 (2002).

[39] N. Felidj, J. Aubard, G. Levi, J. R. Krenn, G. Schider, A. Leitner, and F. R. Aussenegg, Phys. Rev. B **66**, 245407 (2002).

[40] G. Shvets and Y. A. Urzhumov, Phys. Rev. Lett. **93**, 243902 (2004).

[41] S. Y. Park and D. Stroud, Phys. Rev. B **69**, 125418 (2004).

[42] E. M. Hicks, S. Zou, G. C. Schatz, K. G. Spears, R. P. van Duyne, L. Gunnarsson, T. Rindzevicius, B. Kasemo, and M. Kall, Nano Lett. **5**, 1065 (2005).

[43] F. Le, N. Z. Lwin, J. M. Steele, M. Kall, N. J. Halas, and P. Nordlander, Nano Lett. **5**, 2009 (2005).

[44] P. W. Anderson, Phys. Rev. **124**, 41 (1961).

[45] J. Inoue and K. Othaka, J. Phys. Soc. Jpn. **72**, 3024 (2003).

[46] P. Nordlander and F. Le, Appl. Phys. B: Lasers Opt. **84**, 35 (2006).

[47] E. Prodan and P. Nordlander, J. Chem. Phys. **120**, 5444 (2004).

[48] H. Wang, D. W. Brandl, P. Nordlander, and N. J. Halas, Acc. Chem. Res. **40**, 53 (2007).

[49] P. B. Johnson and R. W. Christy, Phys. Rev. B **6**, 4370 (1972).

[50] A. Taflove and S. C. Hagness, *Computational Electrodynamics: The Finite-difference Time Domain Method* (Artech House, Norwood, MA, 2000).

[51] C. Oubre and P. Nordlander, J. Phys. Chem. B **108**, 17740 (2004).

[52] G. Mie, Ann. Phys. **25**, 377 (1908).